Journal of the Mechanical Behavior of Biomedical Materials 171 (2025) 107138

Contents lists available at ScienceDirect

Journal of the Mechanical Behavior of Biomedical Materials

journal homepage: www.elsevier.com/locate/jmbbm

Friction and wear reduction effect of laser powder bed fusion produced Voronoi structures in lubricated metal-polymer sliding pairs

Cong Hou [a,1], István Nemes-Károly [b,1], Leonard Pastrav [a], Bey Vrancken [a,c], Gyorgy Kocsis [d], Gábor Szebényi [b,e,*], Tibor Czigány [b,f], Kathleen Denis [a,**]

[a] KU Leuven, Department of Mechanical Engineering, 3001, Leuven, Belgium
[b] Budapest University of Technology and Economics, Faculty of Mechanical Engineering, Department of Polymer Engineering, 1111, Budapest, Hungary
[c] Flanders Make@KU Leuven, 3001, Leuven, Belgium
[d] Semmelweis University, Department of Orthopaedics, 1082, Budapest, Hungary
[e] MTA-BME Lendület Sustainable Polymers Research Group, 1111, Budapest, Hungary
[f] HUN-REN-BME Research Group for Composite Science and Technology, 1111, Budapest, Hungary

ARTICLE INFO

Keywords:
Voronoi lattice
Ti–6Al–4V
Laser powder bed fusion
Pin-on-disc test
Coefficient of friction
Wear
Joint arthroplasty

ABSTRACT

The failure of artificial joints is often attributed to wear, prompting researchers to explore effective solutions such as material improvement, surface texturing and coating. This study introduces a novel approach of employing 3D printed Voronoi structures to enhance lubrication in polymer-metal sliding wear, with the aim of extending the longevity of artificial joint systems. Specifically, this study investigates the relationship between the geometries and tribological properties of Ti6Al4V Voronoi structures, paired with ultra-high-molecular-weight polyethylene (UHMWPE). The results indicate that the void size in Voronoi structures can be manipulated to match the feature size in the surface texturing approach, suggesting the potential to induce the hydrodynamic effect for friction reduction. The effect of Voronoi structures on reducing friction and wear was examined using pin-on-disc (PoD) tests. In comparison to the control group of solid pins, implementing Voronoi structures in the pins decreases the mean values of static coefficient of friction (COF), dynamic COF, and wear volume by 24.6 %, 29.4 %, and 51.2 %, respectively. Indistinct trends were observed between the COF and the geometric parameters of Voronoi structures. It is hypothesised that interconnected porosity networks within Voronoi structures may preserve wear debris and retain lubricant, potentially elevating hydrodynamic pressure and thereby improving the friction condition. Moreover, comparative analysis of the wear tracks confirms the effective wear reduction achieved by Voronoi structures, with abrasion identified as the primary wear mechanism.

1. Introduction

With the ageing population, the demand for artificial joints, such as shoulder implants, has risen due to the prevalence of age-related joint diseases (Gundersen et al., 2021), (Chen et al., 2019). Shoulder arthroplasty (Fig. 1) typically employ metal-polymer bearing pairs due to their favourable tribological performance and biocompatibility. This configuration typically involves a metallic head component articulating against a polymeric glenoid component (liner) (Al-Shalawi et al., 2023). However, this arrangement presents unique challenges; the shoulder joint's complex range of motion and the relatively small contact area between the head component and glenoid component expose implants to critical wear and friction issues that can accelerate implant failure (Braun et al., 2018). Wear is often initiated by sliding friction on contact surfaces. The resulting wear debris may lead to osteolysis and subsequent bone degeneration. In severe cases, the bone degeneration surrounding the implant can trigger aseptic loosening 10–20 years post-implantation (Harris, 1995), (Connors et al., 2022). Although in

---

* Corresponding author. Budapest University of Technology and Economics, Faculty of Mechanical Engineering, Department of Polymer Engineering, 1111, Budapest, Hungary.

** Corresponding author. KU Leuven, Department of Mechanical Engineering, 3001, Leuven, Belgium

E-mail addresses: cong.hou@kuleuven.be (C. Hou), nemes-karolyi@pt.bme.hu (I. Nemes-Károly), leonard.pastrav@gmail.com (L. Pastrav), bey.vrancken@kuleuven.be (B. Vrancken), kocsisgyorgy@hotmail.com (G. Kocsis), szebenyi@pt.bme.hu (G. Szebényi), czigany@pt.bme.hu (T. Czigány), kathleen.denis@kuleuven.be (K. Denis).

[1] Co-first authors.

https://doi.org/10.1016/j.jmbbm.2025.107138
Received 27 March 2025; Received in revised form 25 June 2025; Accepted 14 July 2025

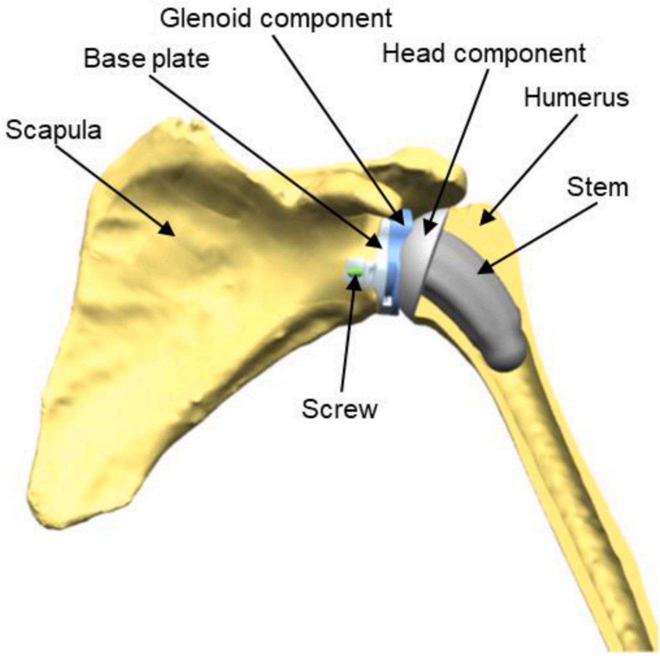

Fig. 1. Bones and artificial components in total shoulder arthroplasty.

vitro wear tests of metal head-polymer liner joints have demonstrated potential lifespans for over three decades, the in vivo lifespan of implanted artificial joints is significantly shorter (Sawano et al., 2009), (Shen et al., 2018).

To mitigate wear, various approaches such as surface texturing and coating have been developed. In 2000, Ito et al. (2000) introduced concave patterns (dimples) on bearing surfaces that serve as reservoirs for wear debris and lubricating fluid. More recently, Choudhury et al. (2018) showed that micro-dimpled surfaces significantly increase lubricant film thickness and promote hydrodynamic lubrication in tribological tests. Subsequent studies discovered that textured surfaces can generate higher hydrodynamic pressures than flat and smooth surfaces, forming a thicker lubricating film between the bearing surfaces (Zhang et al., 2015), (Niu et al., 2021). As an alternative to dimpled structures, Wang et al. (2022) investigated the tribological performance of laser-textured Ti-alloys featuring parallel micro-grooves, reporting markedly reduced coefficients of friction and wear rates compared with non-textured samples. Commonly used texture manufacturing technologies include laser surface texturing (LST), micro-electric discharge machining (Micro EDM), chemical and electrochemical texturing, and additive manufacturing (Lu and Wood, 2020). In particular, Goyal et al. (Goyal and Verma, 2024) showed that Ti6Al4V surface structures fabricated via direct metal laser sintering yielded a 23 % reduction in coefficient of friction and a 68 % decrease in wear compared to bulk material. Moreover, polymer substrates can also be textured. Karunanithi et al. (Karunanithi and Natarajan, 2024) demonstrated that fused-deposition-modeled polyetheretherketone (PEEK) specimens can be produced with controlled surface conditions to tailor their tribological and interfacial properties. In a comprehensive review, Allen et al. (Allen and Raeymaekers, 2020a) highlighted that the tribological properties of surface textures are predominantly determined by their geometric features, such as shape and size. Recent investigations have reported friction reduction of 40 %–50 % and wear reduction exceeding 50 % compared to the untextured surfaces when employing texture sizes ranging from 50 μm to 700 μm and depths varying from 0.5 μm to 100 μm (Niu et al., 2021), (Qiu et al., 2014), (Alvarez-Vera et al., 2021). More information on the tribological behaviour of non-textured metal surfaces can be found in (Nečas et al., 2025). Metals, ceramics, and carbon-based coatings also demonstrated efficiency in reducing wear (Ren et al., 2021), (Zhai et al., 2021). However, the interaction between coating materials and the physiological environment in vivo necessitates consideration, as it can potentially trigger immunological reactions (Łapaj and Rozwalka, 2020).

Tribological properties of materials are commonly evaluated using pre-clinical testing methods such as pin-on-disc (PoD) simulators. In artificial joints, the motion of the head component and bearing component along a single axis can be simplified to the relative motion of a pin sliding against a disc. This allows the interaction between implant components to be simulated using a PoD test setup (Shen et al., 2018). Although PoD tests do not fully capture the multidirectional motion experienced in the shoulder, they offer a straightforward and reproducible method for quantifying key parameters like static and dynamic coefficients of friction (COF) and wear volume. This simplicity makes PoD testing an ideal first step in quantitatively assessing material performance for shoulder implants, prior to more comprehensive joint simulators or in vivo analyses (Kocsis et al., 2018). This quantitative evaluation is important, as the extent of wear in polyethylene components is directly linked to the generation of wear debris. Excessive debris can provoke an adverse immune response, potentially leading to osteolysis, aseptic loosening, and even necessitating revision surgeries. Thus, precise measurement of wear volume not only serves as an indicator of material degradation but also provides critical insights into material's wear performance under conditions of relative sliding motion.

Recent advances in porous materials showed potential for reducing implant wear. Porous materials, such as Oilite®, have been used to improve the tribological condition between mechanical components (Thrush et al., 2021). The interconnected porosity in this material allows for the storage of lubricants, which can be released under pressure to form a fluid film, thereby reducing friction and wear between components. Voronoi structures, a type of random porous structures, exhibit a broad spectrum of mechanical properties (Almonti et al., 2020) and permeability (Zhao et al., 2022) due to their unique and highly customisable geometry. A pilot study conducted by the authors demonstrated the significant potential of Ti6Al4V Voronoi structures in reducing friction against ultra-high-molecular-weight polyethylene (UHMWPE) discs (Hou et al., 2022). Moreover, Odehnal et al. (2025) demonstrated that 3D printed surface structures were capable of retaining albumin within the contact zone and restoring the lubrication film upon unloading, underscoring the lubricant-retention benefits of porous surfaces. Given the unique demands of shoulder implants, this study further explores the tribological properties of Voronoi structures, aiming to identify the relationship between their geometries and tribological properties through comprehensive PoD testing and advanced manufacturing techniques such as laser powder bed fusion (LPBF).

The outcomes of this research are expected to provide original insights into the tribological properties of Voronoi structures. This study addresses whether incorporating Voronoi structures can reduce friction and wear in lubricated metal-polymer sliding pairs, potentially enhancing the designs of current shoulder implants to improve their long-term performance.

2. Materials and methods

2.1. *Design and geometric analysis of Voronoi structures*

Voronoi structures are porous structures that can be generated using random seed points in 3D space (Hanniel and Elber, 2009), (Tanemura et al., 1983). Their geometry can be controlled by two parameters: seed point spacing (SPS), which describes the average distance between the random seed points, and strut diameter (SD), which defines the diameter of Voronoi lattice beams (Li et al., 2023). To fulfil the requirements of PoD tests, pin-shaped Voronoi specimens were designed within a cylindrical boundary with a diameter of 5 mm and a height of 10 mm. The top 2.5 mm comprise Voronoi structures, while the remaining volume was designed as solid bulk material, see Fig. 2 a. To investigate the effect of geometric parameters on tribological properties, Voronoi structures were designated and named based on their "seed point spacing & strut diameter", with numbers in mm. For instance, the structure "0.4&0.2" represents a seed point spacing of 0.4 mm and a strut diameter of 0.2 mm. The geometric parameters of Voronoi structures were employed to ensure that the ranges of relative density (52.8 %–98.5 %, Table 1) encompass those of Oilite®, and feature sizes approximate those of surface texturing designs. The relative densities (volume ratios) of the Voronoi structures were calculated by dividing the volume of the Voronoi structure by the volume of the cylindrical boundary, using only the data from the top 2.5 mm height of the CAD geometries.

The geometry and morphology of Voronoi structures play significant roles in their tribological behaviour. The unique characteristics of Voronoi structures, such as their high porosity and complex micro-architectures, can influence the contact mechanics between the structures and bearing components. Unlike surface texturing designs, which generate surface patterns on solid parts, Voronoi structures possess volumetric porosities. This unique feature facilitates both the flow and storage of lubricant within the structure. Besides, the contact area between the bearing components directly affects the load distribution and local deformation, thereby affecting the friction and wear properties (Williams, 2005), (Kim, 2022a). The surface of Voronoi structures exhibits polygon-shaped textures, which are referred to as voids and measured from section images generated at the midpoint of the top layer struts (see the green section plane in Fig. 2 a and b). The images were subsequently binarised using ImageJ (National Institutes of Health, MD, US). The contact area was determined based on the count of black pixels (see Fig. 2 c), while the voids were identified and measured from the binary image (see Fig. 2 d) using a MATLAB (The MathWorks Inc, MA, US) script. The equivalent diameter of voids is defined as the diameter of circles with identical areas. The pixel-based contact area and void information were further analysed and summarised using an R script (R Core Team and R, 2021).

2.2. *Manufacturing and characterisation of Voronoi structures*

Ti6Al4V powder (grade 23, Carpenter Additive, UK), featuring particle sizes ranging from 15 to 53 μm, was used to manufacture three specimens of each Voronoi structure using a ProX 320B laser powder bed fusion (LPBF) system (3D Systems, Belgium). The employed process parameters (Hou et al., 2024) are shown in Table 2. The specimens were subsequently removed from the build plate using wire Electric Discharge Machining (EDM) and subjected to cyclic ultrasonic cleaning in water and ethanol to remove powder residues.

Following manufacturing, the specimens were analysed using a scanning electron microscope (SEM, XL30 FEG, FEI Company, The Netherlands). To ensure a flat and smooth surface and parallel surface alignment between the Voronoi specimens and the UHMWPE discs in the subsequent tests, the top surface of the pins was polished using a Buehler Beta device (Buehler, Germany) with wet 300- and 1000-grit polishing papers (see Fig. 2 e and f). Subsequently, the top surfaces of the Voronoi specimens were observed and analysed using an optical microscope (Keyence VHX-5000, Keyence, Japan). The void sizes on the top surfaces were detected and measured based on the optical microscope images, using the same methodology described in Section 2.1 (see Fig. 2 g and h).

2.3. *Tribological test and analysis*

UHMWPE discs, serving as the bearing components, were machined from 30 mm diameter UHMWPE rods (GUR 1020 medical-grade, Mitsubishi Chemicals Advanced Materials, Germany). The discs were initially cut, followed by surface polishing using a Buehler Beta device (Buehler, Germany). Wet polishing was conducted using 300- and 1000-grit polishing papers. The specimens underwent a 5-min polishing process on each paper to achieve a uniform and low-roughness surface finish. Following preparation, the surfaces of the polymer discs were evaluated to ensure the quality and consistency of the polishing process.

A PoD tribometer (TRB3, Anton Paar GmbH, Austria) was used to determine the tribological properties between the Ti6Al4V pins and the UHMWPE discs, see Fig. 3 a. The experimental protocol was designed in accordance with ASTM G99-17 (Standard Test Method for Wear and Friction Testing with a Pin-on-Disk or Ball-on-Disk Apparatus), and the testing parameters were adapted to align with loading conditions of artificial shoulder joint, see Table 3. Before testing, the UHMWPE discs were fixed into the disc holder, and the Voronoi specimens were installed in the pin holder, see Fig. 3 b. Three solid Ti6Al4V cylindrical pins, following the same preparation procedure, were used as the control group. Bovine serum, obtained from young cattle, was used as the synovial fluid and added to the fluid reservoir. A constant load of 20 N was applied on the top of the pin holder. When this load is distributed on the surface of the pin (with a 5 mm diameter), it produces an average pressure of 1.0 MPa. This value was selected to reflect the in vivo conditions of the shoulder joint. For context, for a 50th percentile male weighing 87.4 kg (Fryar et al., 2021), lifting a 2 kg weight generates a

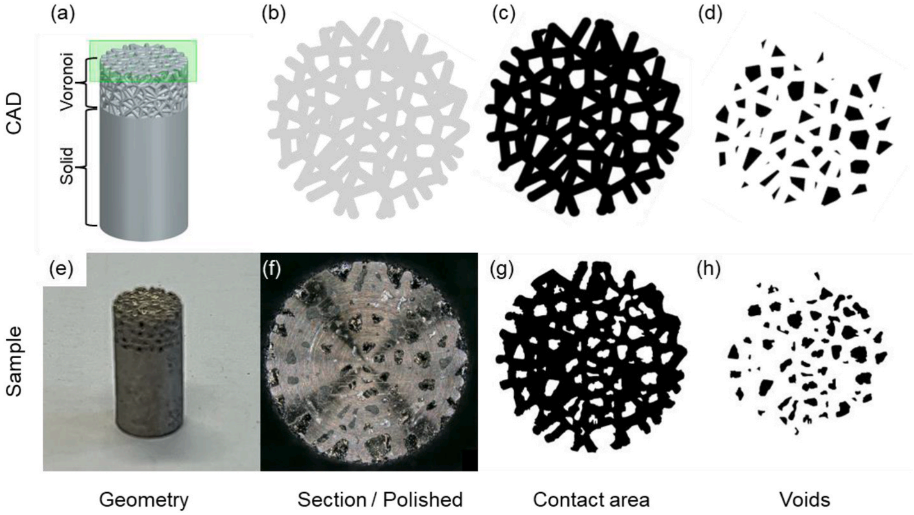

Fig. 2. Schematics of Voronoi structures (a), (e), section images (b), (f) and binarised images of CAD geometry (c), (d), and sample (g), (h). The structure shown is "0.5&0.25". Binarised images are used to measure contact areas and surface features.

Table 1
Relative density of Voronoi structures in percentage, with the indication of seed point spacing and strut diameter. A dash (–) indicates such geometry was not employed.

Relative density (%)		Seed point spacing, SPS (mm)					
		0.22	0.3	0.4	0.5	0.6	0.7
Strut diameter, SD (mm)	0.2	98.5 %	93.1 %	68.5 %	52.8 %	–	–
	0.25	–	96.4 %	84.0 %	67.8 %	54.6 %	–
	0.3	–	–	96.2 %	80.3 %	67.3 %	55.6 %
	0.35	–	–	96.4 %	90.8 %	77.3 %	67.3 %

Table 2
LPBF parameters for manufacturing Voronoi pins.

Laser parameters	Laser power	45 W
	Laser scan speed	300 mm/s
	Laser beam diameter	90 µm
Scan strategy	Layer height	30 µm
	Number of contours	3
	Hatch	50 µm

physiological load of approximately 1045 N (Bergmann et al., 2011), equivalent to around 122 % of body weight. When this force is applied over an average glenoid surface area of 959.4 mm^2 (Misir et al., 2019), the resulting mean pressure is 1.1 MPa. Consequently, the 20 N test load was used to approximate the physiological pressure encountered in shoulder joint applications. All specimens underwent an 8-h testing process using the configuration specified in Table 3.

Throughout the tests, the linear unit facilitated the bidirectional movement of the disc holder, while the motion and friction force were continuously recorded by the position sensor and load cells. Fig. 3 c illustrates how COF changes during a single test cycle. The static COFs are defined by the peak values within their specific stroke ranges, and the dynamic COFs are calculated as the average values within their corresponding stroke ranges. After testing, the UHMWPE discs were sputter-coated with gold using a JEOL FC 1200 (Jeol, Japan) device to achieve a conductive surface, followed by observation using a JEOL JSM 6380LA (Jeol, Japan) SEM. This method not only reveals the morphology of the wear track but also facilitates the assessment of contact conditions during testing, thereby enabling the identification and exclusion of any data arising from uneven contact or misaligned pin installation. The wear tracks on UHMWPE discs were then scanned using a Keyence VR6000 3D Optical Profilometer (Keyence, Japan), which provided detailed 3D imaging data. A reference surface was selected on the unworn area of each disc, and the wear volume was calculated relative to this reference, yielding a quantitative measure of the wear volume. Finally, the results of the PoD tests were further analysed using an R script (R Core Team and R, 2021).

3. Results

3.1. LPBF manufacturing of Voronoi structures

Fig. 4a–h shows SEM images of Voronoi structures. Struts are visible in the more porous structures, albeit with imperfect cylindrical shapes. In contrast, the struts in the denser structures are less distinct and barely recognisable. A large number of adherent particles can be identified on the strut surfaces. Small voids have been filled during the LPBF manufacturing (A in Fig. 4 f). Fig. 4 g shows higher magnification SEM images of the marked area on the structures “0.5&0.25”. Defects at strut junctions, appearing as holes (B and C), were also observed. Fig. 4 j and k illustrate the LPBF trajectories of the second last layer for the Voronoi structure “0.5&0.25”, with corresponding locations displayed in insets f and g. The comparison of SEM images and laser trajectory shows that the strut geometry correlated closely with the location and shape of the laser passes: a high density of trajectories locate around the filled small voids (A in Fig. 4 j), whereas defect locations correspond to blank areas lacking laser pass (B and C in Fig. 4 k) at strut junctions. The CAD models of structures “0.5&0.25” and “0.4&0.35” are illustrated in insets i and l, respectively. The top surfaces of the structures are highlighted in green. A comparison between the CAD models and SEM images reveals that dense structures demonstrate poorer geometric accuracy than the porous structures, with many barely recognisable struts and numerous defects after the LPBF process.

3.2. Geometric characterisation of Voronoi structures

Fig. 5 and Table 4 (appendix) summarise the analysis of voids and contact areas within Voronoi structures. Although the geometric properties of the voids measured from both CAD geometries and specimens differ, they display similar tendencies. As the seed point spacing decreases or the strut diameter increases, the Voronoi structure densifies, exhibiting a surface morphology that resembles the dimples found in conventional surface texturing approaches (see Fig. 4). This observation suggests a potential to improve tribological conditions. However, in contrast to the round dimples typical of surface texturing, the voids on the CAD models of Voronoi structures are polygonal. Following manufacturing and subsequent polishing, the voids exhibit irregular shapes and dimensions that deviate from the intended design (see Figs. 5 and 2 d and h). Fig. 5 a presents the equivalent diameters of voids in different Voronoi structures, in relation to seed point spacing (SPS) and strut diameter (SD). Unlike the uniform feature size observed in most typical surface textures, the voids in Voronoi structures fall within specific size ranges. The void dimensions in specimens are larger than those in the CAD designs, correlating positively with seed point spacing and negatively with strut diameter. Fig. 5 b shows scatter plots of the voids' aspect ratios with respect to equivalent diameter. While many small voids are elongated, larger voids tend to be nearly circular. Fig. 5 c illustrates the distribution of equivalent void diameters relative to the distance from the void centre to the structure's central axis (“distance to centre” in inset c), confirming that the void size is independent of their location on the surface of Voronoi structures, which is expected due to the inherent randomness of the Voronoi cells. Furthermore, the contact area between the Voronoi structure and the bearing component increases with strut diameter (SD) and decreases with seed point spacing (SPS), Fig. 5 d.

3.3. Correlation between tribological properties and geometries of Voronoi structures

The PoD test results (see Figs. 6 and 7 and Table 4 in appendix) shows that Voronoi structures exhibited improved tribological properties compared to the control group. Using Voronoi structures significantly reduces static COF, dynamic COF, and wear volume (Fig. 6 a). The static COF reduced from 0.24 ± 0.01 to 0.18 ± 0.05, the dynamic COF reduced from 0.22 ± 0.02 to 0.15 ± 0.04, and the wear volume reduced from 1.14 ± 0.10 mm^3 to 0.56 ± 0.24 mm^3. All reductions are statistically significant (p-values <0.01). However, the boxplots that compare individual Voronoi structures with the control group (Fig. 6b–d) reveal that the effect of seed point spacing on these tribological properties is not consistent. For instance, structures with strut diameters of 0.2 and

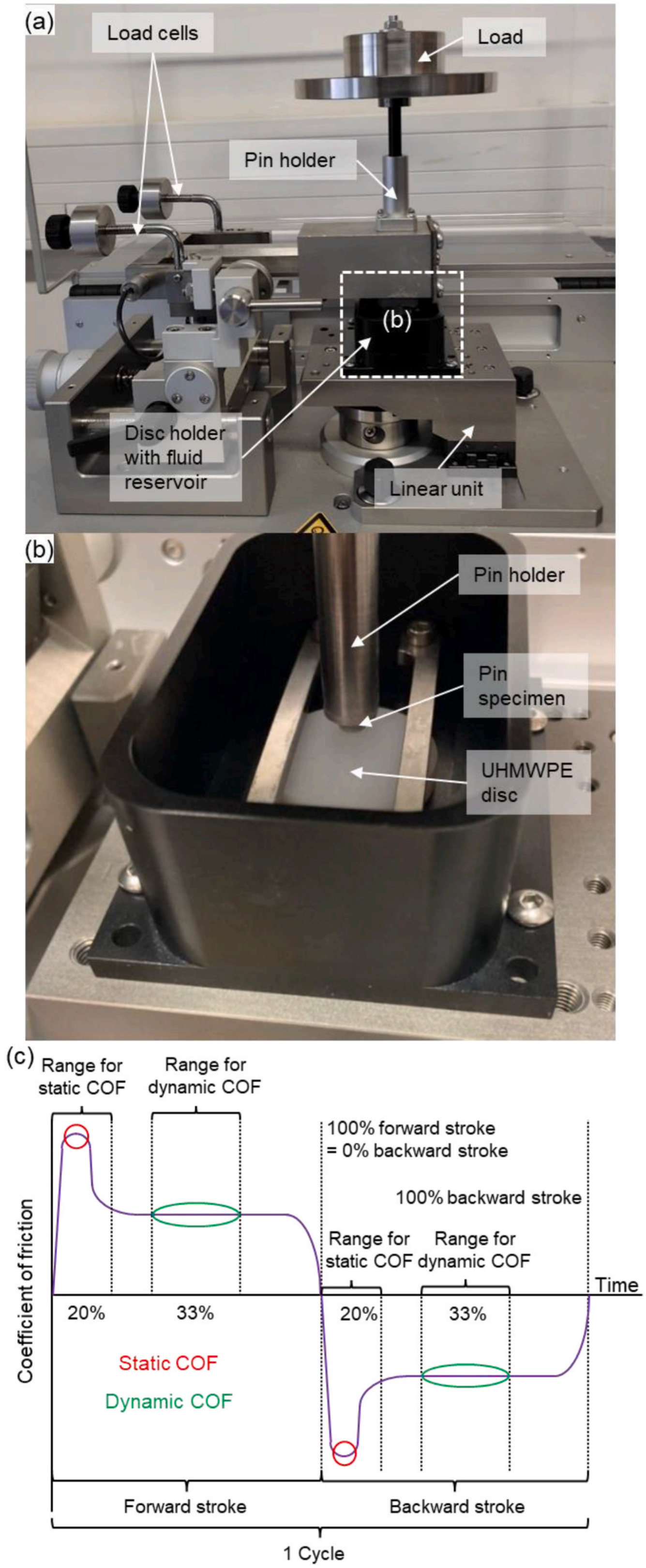

Fig. 3. The methodology of tribological tests. (a) The TRB3 PoD tribometer, with the configuration of installed Voronoi specimens and UHMWPE disc (b). (c) The methodology for evaluating the static and dynamic coefficient of friction.

Table 3
Testing parameters of TRB3 PoD tribometer.

Movement amplitude (oscillation)	20 mm
Frequency	1 Hz
Load	20 N
Data acquisition rate	80 Hz
Test period	8 h

0.3 mm generally show increased static and dynamic COF, as well as wear volume, with increasing seed point spacing, whereas the structures with the other two strut diameters tend to exhibit a decrease in friction coefficients and wear volume. Similarly, variations in strut diameter have non-uniform effects on the tribological properties, with some cases displaying minimal variation and others showing fluctuations. Besides, the scatter plots in Fig. 7 reveal that the tribological properties do not exhibit any consistent trends with respect to void size, contact area, and relative density.

These observations suggest that the influences of seed point spacing, strut diameter, void size, contact area, and relative density on the tribological properties are complex and may be minimal. The variability observed in the boxplots and scatterplots indicates that no clear, consistent effect is discernible without a more detailed statistical analysis.

Fig. 8 illustrates the correlation coefficients between various geometric and tribological parameters, with the specific values of correlation coefficients and their corresponding p-values presented in Tables 5 and 6 (appendix). This analysis reveals that the correlation coefficients between geometric parameters (seed point spacing, strut diameter, relative density, void size, contact area) and tribological properties are close to zero, aligning with the observations in Figs. 6 and 7. None of these correlations are statistically significant (Table 6). In contrast, relative density, void size and contact area show stronger correlations with seed point spacing, reflecting the strong correlations observed in section 3.2. Importantly, the tribological properties (static COF, dynamic COF, and wear volume) display strong correlations among themselves, indicating that reduction in friction (i.e. reduced COF) is strongly associated with decreased wear. While some vague tendencies between the tribological properties and geometric parameters were observed, statistical analyses, incorporating linear, interaction, and polynomial terms, failed to reveal significant effects. All statistical models yielded low R^2 values and non-significant p-values for all terms.

Fig. 9 illustrates the wear morphology of UHMWPE disc surfaces. The relative motion between the pins and discs is in the horizontal direction. The pins used in the comparison include solid pins (control) and Voronoi pins with various combinations of seed point spacing and strut diameter. The wear track of the control group shows massive material removal in the middle of the test stroke (Fig. 9 a, left inset), with the maximum local material removal reaching 23 μm. On the contrary, the wear track of a Voronoi sample (Fig. 9 a, right inset) shows much less (maximum 18 μm) and more homogeneous material removal. Fig. 9 b shows detailed wear surfaces of UHMWPE discs, observed using SEM. The control group exhibited a significant material loss, with numerous deep furrows aligned with the sliding direction and variable wear debris dimensions. In contrast, discs tested with the Voronoi pin demonstrated smoother surfaces, shallower furrows, and fewer wear debris particles partly attached to the surface. At high magnification, light-coloured staircase-like features appear on both types of discs, potentially indicating subsurface cracks and delamination. Fig. 10 illustrates the surface morphology of the Ti6Al4V Voronoi pins before and after PoD tests. Post-test examination revealed the formation of distinct furrows on the pin surface, demonstrating material removal resulting from frictional contact during cyclic relative motion, potentially caused by third-body wear.

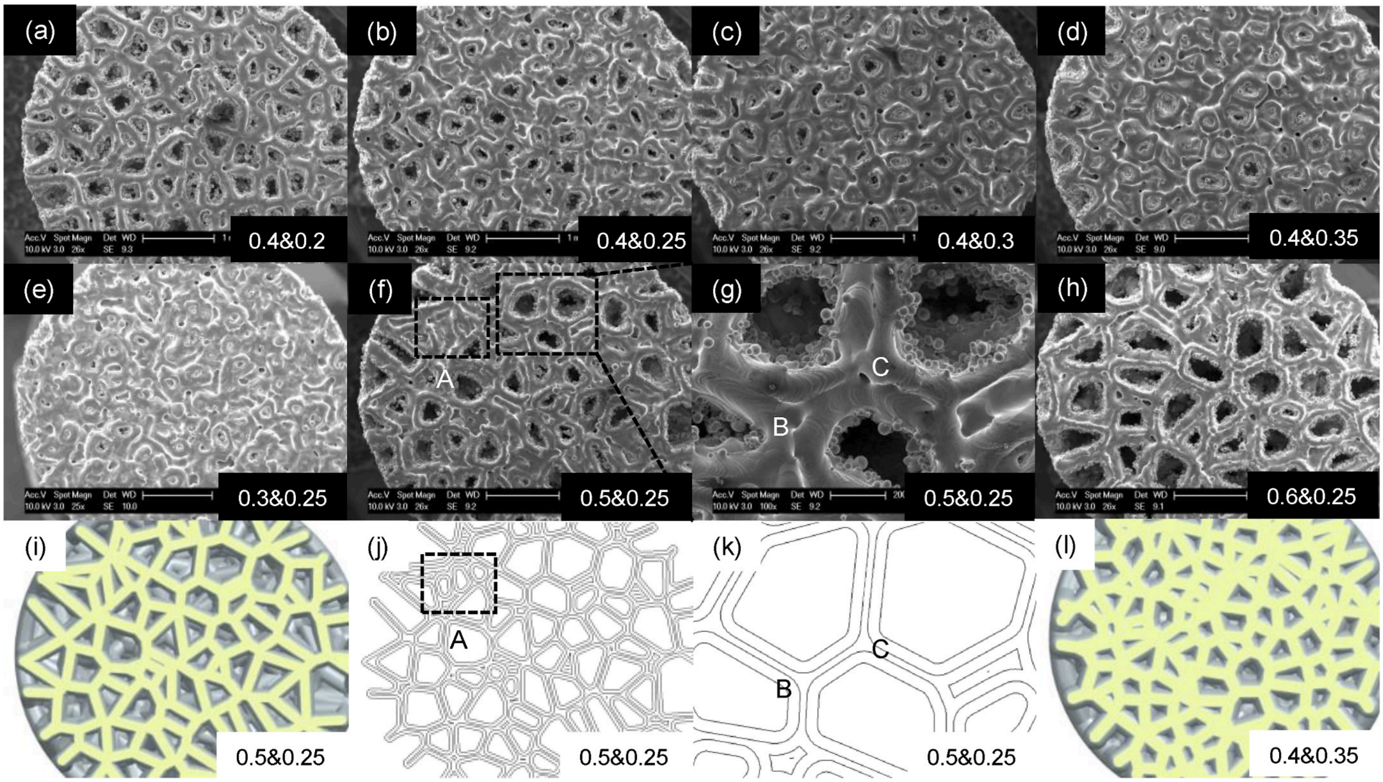

Fig. 4. (a–h) SEM images of Voronoi specimens, with indications of seed point spacing and strut diameters. (j–k) Laser trajectories for the structure "0.5&0.25", CAD geometries for the structures (i) "0.5&0.25" and (l) "0.4&0.25".

4. Discussion

4.1. Evaluation of manufacturing quality

The limited geometric accuracy of strut shapes can be primarily attributed to the particular thermal conditions encountered when printing thin-strut lattice structures. Owing to the limited capacity to dissipate heat from the melt region, the solid material experiences localised overheating. This results in adjacent powder particles partially sintering to the strut (Zhang and Li, 2022) and an increased melt pool size, which in turn leads to an overprinting of the intended dimensions and higher-than-designed relative densities. This issue can be accommodated by selecting appropriate process parameters and scan strategies. In particular, for denser structures, the overprinting may lead to the closure of small voids and fragmentation of the pore network into isolated volumes. Such an absence of voids may limit the development of hydrodynamic pressure during PoD tests and thus worsen the frictional condition. Moreover, the sintered powder particles are a cause of concern, as there is fear that they can detach and function as hard particles in abrasive wear. Process parameter optimisation may reduce their initial occurrence (Xue et al., 2023), and subsequent removal using electrochemical cleaning is also possible (Liu et al., 2022).

Numerous holes were observed at the strut junctions, corresponding to unscanned or blank areas during the LPBF process (B and C in Fig. 4 g), which can be ascribed to the parameters employed in the scan strategy (Fig. 4 k), including the number of contours and hatch values. Such defects can be mitigated by further optimising the LPBF parameters and strategies, as described in a previous study by the authors (Hou et al., 2024).

4.2. Adaptive geometry of Voronoi structures

Surface texturing has demonstrated efficacy in mitigating friction and wear between bearing components (Lu and Wood, 2020). As shown in Figs. 2 and 4, the voids on the surfaces of Voronoi structures resemble the features in surface texturing. The void sizes and contact areas are directly related to the geometry of Voronoi structures, specifically the dimensions and distributions of the struts. The edges of a void are defined by the surrounding struts. Thus, higher seed point spacing and/or lower strut diameter leads to longer and/or thinner struts, resulting in a more porous structure. Consequently, the voids exhibit greater edge length and area, and the overall contact area is reduced. In both the CAD geometries and the specimens, most void sizes range from 0.05 mm to 0.5 mm (Fig. 5 a), falling within the range of the commonly used dimple sizes in surface texturing approaches (Shen et al., 2018). Consequently, these dimple-like voids may offer similar functions, such as hydrodynamic effects (Allen and Raeymaekers, 2020a), retaining lubricants and trapping wear debris, thereby collectively enhancing tribological performance.

The deviations in the void shapes and dimensions observed in the specimens (compared to CAD) can be attributed to two main factors. Firstly, the inherent limitations of the LPBF process affect the geometric accuracy. As discussed in section 3.1, the interaction between the powder material and the laser spot can lead to struts that do not perfectly replicate the intended design, while residual stress can further deform the struts geometry (Wu et al., 2020). Secondly, the manual polishing process, primarily controlled by the polishing duration, may lead to inconsistent local material removal. As a result, in one specimen, the material removal may be greater in some areas than in others. This lack of precise control over the polishing depth could result in deviations in the dimensions and shapes of the voids.

The near-homogeneous distribution of equivalent void diameters with respect to their distance from the central axis (Fig. 5 c) underscores the high degree of geometric randomness of Voronoi structures, potentially contributing to quasi-isotropic behaviour. By adjusting seed point spacing and strut diameter, one can modify geometric properties such as relative density, void size, and contact area in Voronoi structures, thereby offering significant flexibilities in design and optimisation.

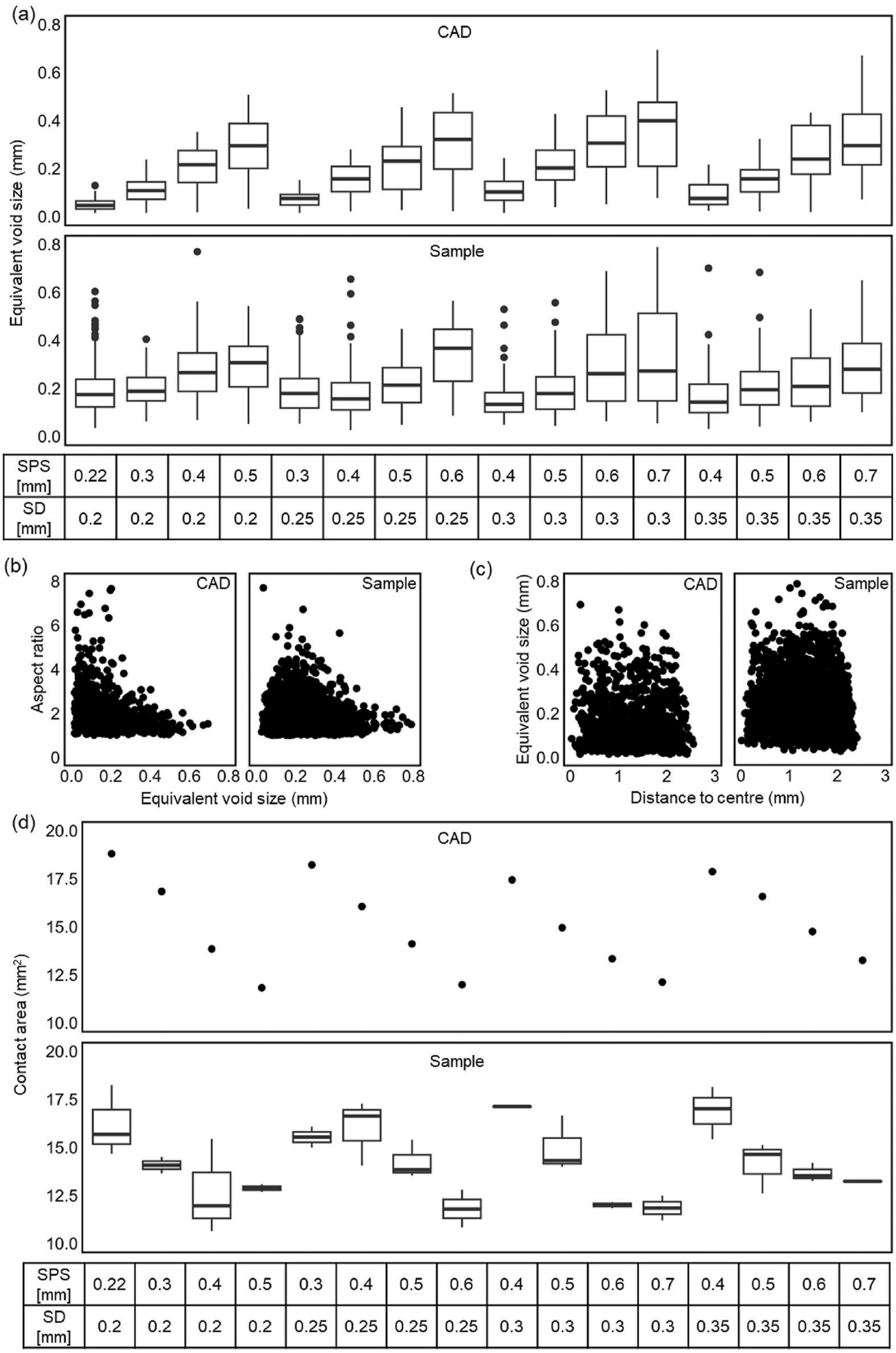

SPS [mm]	0.22	0.3	0.4	0.5	0.3	0.4	0.5	0.6	0.4	0.5	0.6	0.7	0.4	0.5	0.6	0.7
SD [mm]	0.2	0.2	0.2	0.2	0.25	0.25	0.25	0.25	0.3	0.3	0.3	0.3	0.35	0.35	0.35	0.35

SPS [mm]	0.22	0.3	0.4	0.5	0.3	0.4	0.5	0.6	0.4	0.5	0.6	0.7	0.4	0.5	0.6	0.7
SD [mm]	0.2	0.2	0.2	0.2	0.25	0.25	0.25	0.25	0.3	0.3	0.3	0.3	0.35	0.35	0.35	0.35

Fig. 5. Geometric analysis results of Voronoi structures, including (a) equivalent diameter of voids, (b) aspect ratio of voids, (c) distance to centre of voids and (d) contact area of Voronoi structure, for both CAD geometries and measured data of the printed specimens. Seed point spacing (SPS) and strut diameter (SD) for each group of specimens are shown at the bottom of the insets.

4.3. Significantly improved tribological properties of Voronoi structures

Friction in the PoD tests encompasses multiple mechanisms. During cyclic motion, tribological conditions alternate between static friction, when the sliding direction reverses, and dynamic friction, which occurs during continuous sliding. According to Amonton's and Coulomb's laws, the friction force comprises an adhesive component and a deformation component (Kim, 2022a). At the end of each test stroke, the speed of the linear unit reduces to zero, thus fulfilling the conditions for the pre-sliding regime (static friction). In this case, the friction force is predominantly adhesive, primarily caused by the interlocking asperities at local contact points of the material at nanoscale (Hanaor et al., 2016).

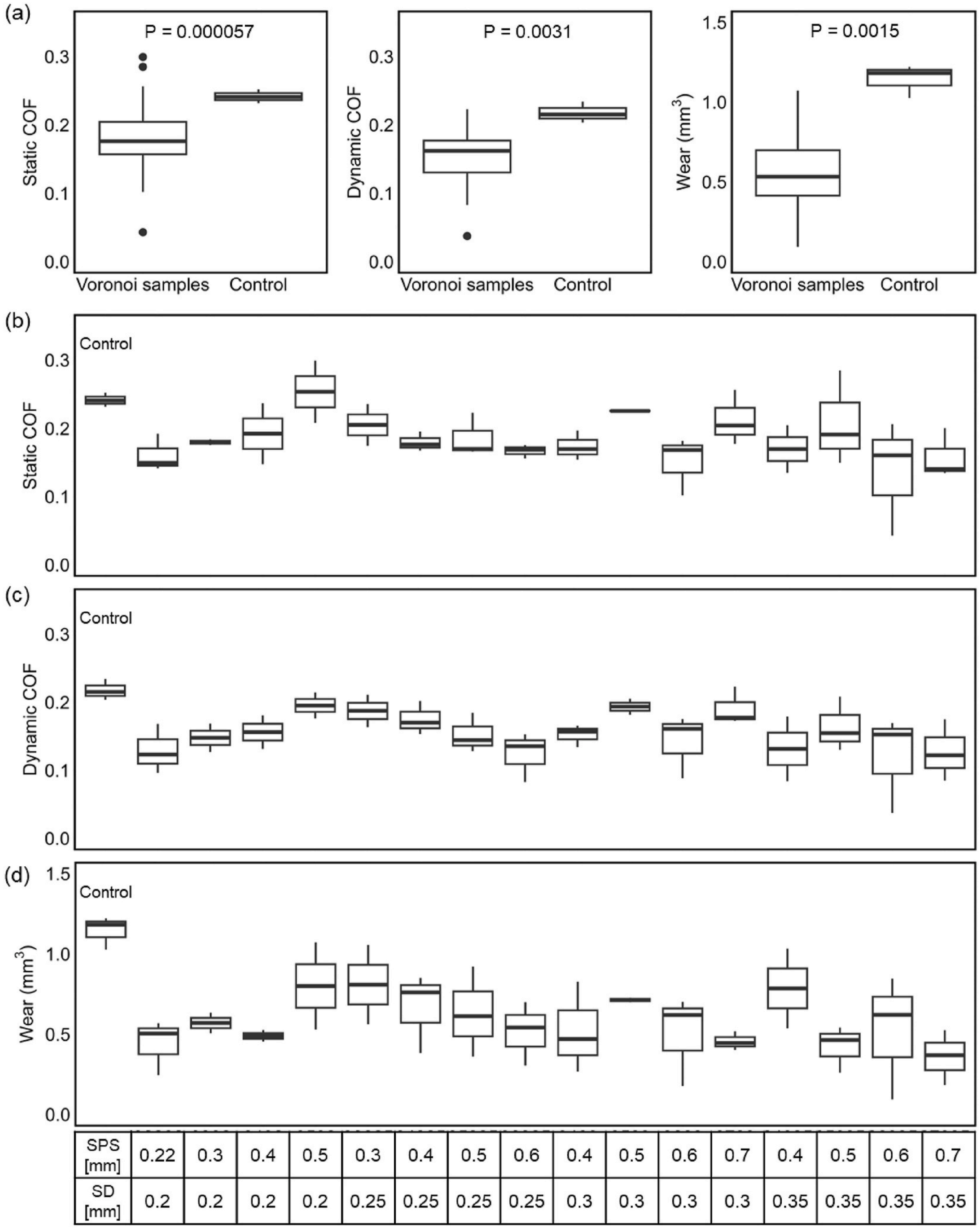

SPS [mm]	0.22	0.3	0.4	0.5	0.3	0.4	0.5	0.6	0.4	0.5	0.6	0.7	0.4	0.5	0.6	0.7
SD [mm]	0.2	0.2	0.2	0.2	0.25	0.25	0.25	0.25	0.3	0.3	0.3	0.3	0.35	0.35	0.35	0.35

Fig. 6. Tribological properties of the Voronoi specimens compared to the control group, including static and dynamic coefficient of friction (COF) and wear volume. The p-values represent the significance of the differences. Seed point spacing (SPS) and strut diameter (SD) for each group of specimens are shown at the bottom of this figure.

As displacement increases, the local interlocks break, transitioning the pre-sliding regime to the gross-sliding regime (dynamic friction) (Kim, 2022b). With increasing speed, the lubricant film thickens, and the lubrication mode gradually transitions from boundary lubrication to mixed lubrication, and finally to hydrodynamic lubrication. In the case of hydrodynamic friction, the lubricant film separates the surfaces. Consequently, the dynamic friction can be significantly lower than static friction (Burstein, 2011).

Wear in PoD tests results from a combination of adhesive wear, abrasive wear, and surface fatigue wear due to the interactions between the Voronoi pin, UHMWPE disc, and synovial fluid (Ajimotokan, 2024). Adhesive wear occurs when asperities are compressed together and form local bonds. The material on one surface undergoes plastic deformation, shearing, and adherence to the other surface during relative motion. The adherent material is eventually released into the lubricant and forms debris. Abrasive wear occurs when hard asperities or particles penetrate a softer surface, causing material deformation and removal. This process results in grooves, scratches, or indentations on the softer surface, as seen in Fig. 9 a. The severity of abrasive wear is influenced by factors such as the hardness difference between the two materials, the shape and size of the hard particles, and the applied load. Fatigue wear occurs when a surface is subjected to cyclic loadings, which can cause cracks to initiate and propagate beneath the surface. Over time, these cracks can reach a critical size and cause fragments of material to detach, resulting in pits and wear on surfaces (Kim, 2022b), (Jiménez and Bermúdez, 2011). When debris is present, third body wear can occur. In

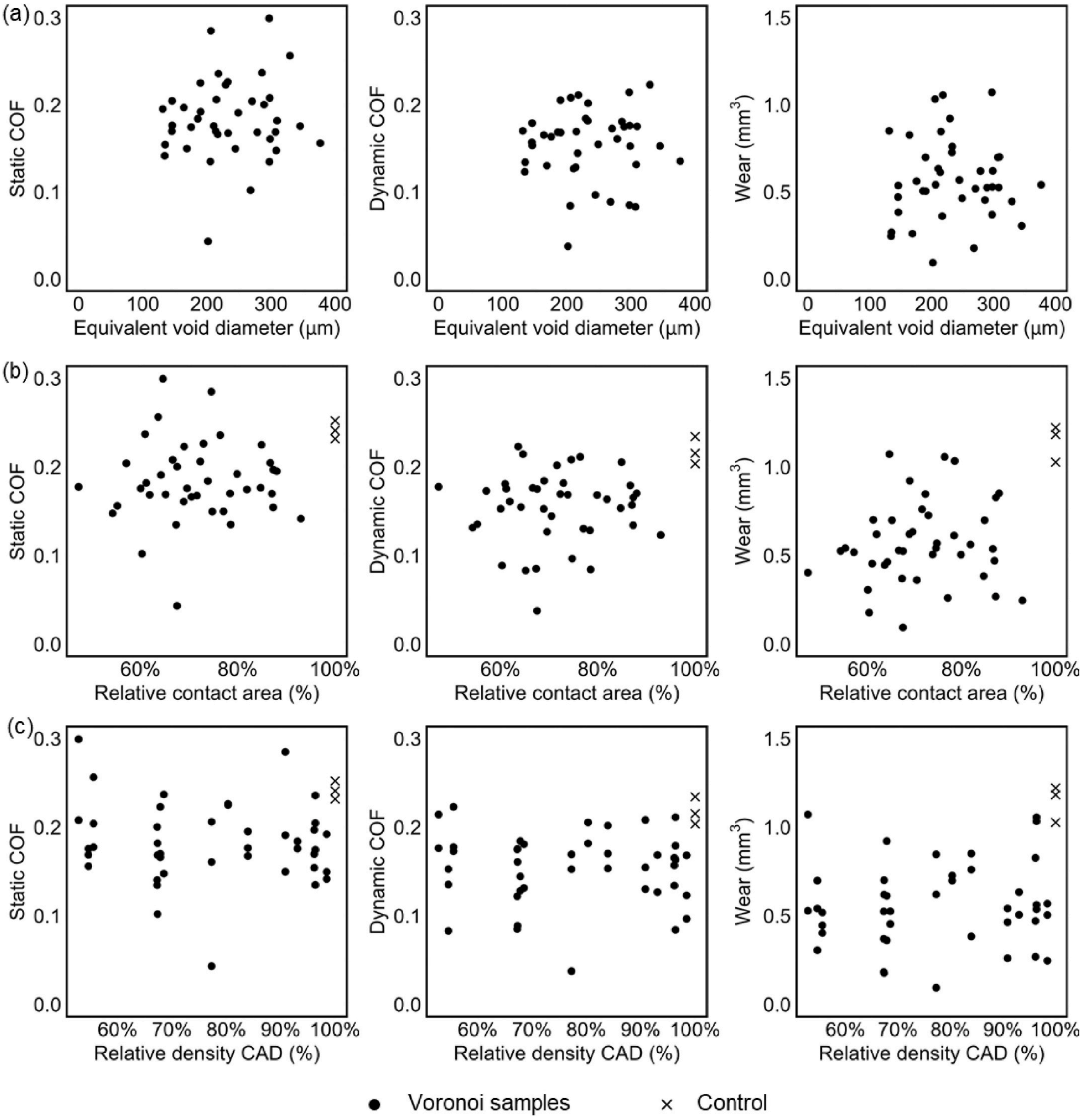

Fig. 7. Tribological properties versus void size (a), contact area (b) and relative density of CAD models (c).

LPBF-fabricated parts, the trapped or weakly bonded powder can also increase third body wear, making effective cleaning and post-processing essential.

Consequently, strategies for friction and wear reduction may focus on minimising adhesive forces between surface pairs, enhancing fluid film thickness, addressing hardness difference between surfaces, as well as managing hard particles and debris.

The significant reductions in static COF, dynamic COF, and wear volume (Fig. 6 a) are attributed primarily to the high porosity of Voronoi structures, which enhances tribological conditions between the Voronoi pins and the UHMWPE disc through three key mechanisms:

1. Enhanced fluid retention:

The interconnected pores in Voronoi structures preserve a large volume of synovial fluid via the capillary effect, which is determined by parameters such as porous material morphology, temperature, and fluid properties (Chen et al., 2022). In contrast to surface texture approaches where synovial fluid may be preserved within dimples on the specimen surfaces, Voronoi structures exhibit superior fluid retention due to their high porosity throughout the entire volume and the resulting capillary effect. Analogous to the mechanism of surface texture and Oilite® components, the remaining synovial fluid within the Voronoi structures can adhere to the specimen surfaces during the relative motion between

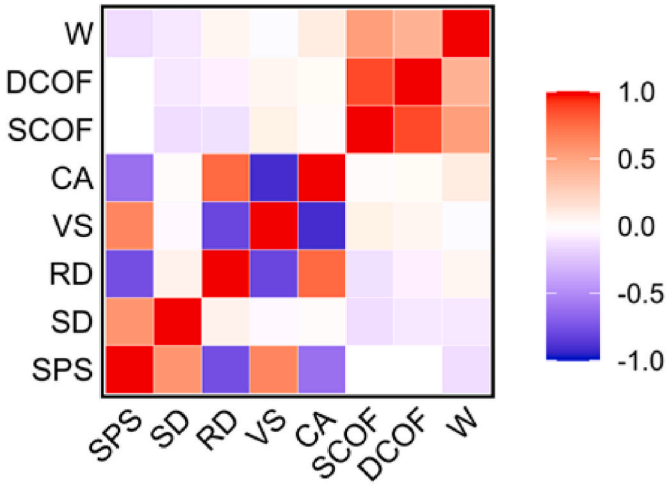

Fig. 8. Correlation coefficients of parameters: seed point spacing (SPS), strut diameter (SD), relative density (RD), equivalent void diameter (void sizes, VS), contact area (CA), static coefficients of friction (SCOF), dynamic coefficients of friction (DCOF), and wear volume (W).

the pins and discs. The induced hydrodynamic pressure increases the lubricant film thickness, thereby forming a more stable film that effectively separates the bearing surfaces (Allen and Raeymaekers, 2020b). Thus, the adhesive force between the surfaces is reduced, and the lubrication mode is transferred from boundary lubrication to full film lubrication (Ajimotokan, 2024), (Stewart, 2010). A similar phenomenon was recently reported by Odehnal et al. (2025), where surface structuring of additively manufactured Ti6Al4V pins enhanced lubricant retention and promoted albumin retention during tribological testing, thereby improving lubrication conditions. Besides, the cyclic motion between the pin and disc can lead to fatigue wear. Thicker lubricant film can help reduce fatigue crack initiation and avoid failures under cyclic load (Abdelbary, 2021).

2. Debris entrapment:

The porosity of Voronoi structures can trap small wear debris, which typically act as third bodies to scratch and plough the soft surface (Shen et al., 2018). Surface texture approaches employ concave patterns to retain debris (Wei et al., 2016). Similarly, the high volumetric porosity in Voronoi structures also facilitates debris entrapment. This feature consequently mitigates the damage and material loss in the third body wear. Besides, wear debris may trigger several adverse biological reactions in periprosthetic tissues, such as inflammatory response and osteolysis. These effects progressively compromise the integrity of bone and soft tissue, making them unable to support implants. In severe cases, this leads to implant instability, also known as aseptic loosening (Nine et al., 2014). Voronoi structures' ability to wear debris gathering reduces such risk.

3. Polymer debris embedment:

Polymer debris with certain sizes may become firmly embedded in the voids due to their dimensions aligning with the void size, as shown in Fig. 11. The embedment partially transforms the original metal-polymer sliding pairs to polymer-polymer sliding surfaces. Since softer materials are prone to greater wear when paired with harder materials (Zhai et al., 2021), this embedment reduces the effective hardness and stiffness mismatch between the contact surfaces, thereby further reducing the wear rate.

Evidence for debris embedment is provided by observations in Fig. 11. The polymer fragment sizes in the insets, measuring several hundred microns, correspond well with typical wear debris dimensions (Shen et al., 2019) and aligns with the void size (Fig. 5 a), making embedment plausible. In sliding wear tests, larger debris tend to become embedded into bearing surfaces while smaller ones are more likely to be carried through the contact area (Shen et al., 2019). The top inset in Fig. 11 illustrates evidence of prolonged interaction between the embedded debris and the environment, as part of the debris appears worn away during the continued sliding contact. In contrast, the largely intact debris in the bottom inset likely reflects a shorter interaction period before the end of the test. Additionally, the perfect fit of the debris within the void can be attributed to the elastic deformation of the polymer debris under 8-h cyclic loading, which allows the softer polymer to conform gradually to the geometry of the metal cavities (voids). These observations confirm the wear debris embedment, which mitigates stiffness mismatches and reduces the wear rate.

While employing Voronoi structures significantly reduces the COF and wear volume, the influence of the geometric parameters (such as strut diameter, seed point spacing, equivalent void diameter, contact area and relative density) on the tribological properties appears limited (Figs. 6 and 7). Statistical analysis did not reveal significant correlations between the geometric parameters and tribological performance (Fig. 8, Tables 5 and 6). One possible explanation is that the presence of a porous architecture itself may be the dominant factor driving the observed improvements, with the precise feature sizes – at least within the investigated range of designs – playing a secondary role. Additionally, three main limitations may have contributed to the lack of detectable trends. Firstly, the variation in the geometric parameters among different Voronoi structures is minimal. As demonstrated in Section 3.2, the void size ranges across various Voronoi structures exhibit high overlaps (Fig. 5 a), suggesting that the aforementioned mechanisms in many structures can be achieved to a similar extent. Secondly, only three specimens per sample were tested. This relatively small sample size may hinder the detection of subtle effects and potentially increase the risk of bias (Serdar et al., 2021). Thirdly, the relatively short testing duration may not be sufficient to detect long-term differences in tribological properties. Future studies should consider broader geometric variations, larger sample sizes, and extended testing periods to better resolve these limitations. Furthermore, using testing methods such as joint simulators enables replicating the intricate motion and loading conditions experienced in vivo (Shen et al., 2019), which can also mitigate the strain-hardening effect of the UHMWPE discs due to uniaxial motion in PoD tests and offer more representative results for further applications. Future work could also consider using optical interferometry to quantitatively evaluates the hydrodynamic behaviour introduced by porous Voronoi structures (Odehnal et al., 2025).

The wear surfaces of UHMWPE discs observed in the PoD tests align with fundamental tribological principles. The deep furrows on the surfaces in the control group (Fig. 9) confirm abrasive wear as the dominant mechanism, where hard asperities or debris ploughed into the polymer surface, leading to material removal through micro-cutting and grooving. This aligns with the discussion that interfacial hardness mismatch and hard particles critically influence abrasive wear severity. In contrast to the control group, the discs paired with Voronoi pins demonstrated reduced furrow depth and material loss, suggesting that the porous Voronoi structure potentially trapped wear debris within its interconnected pores, thereby mitigating third-body abrasion. This improvement is similar to the wear reductions observed on the UHMWPE surfaces when using surface texturing approaches (Alvarez-Vera et al., 2021). Staircase-like features on disc surfaces correlated with fatigue wear, driven by cyclic loading and relative motion that promotes subsurface crack initiation and localised accumulations of plastic deformation (Igual Munoz et al., 2020). Over time, delaminated material of small dimensions could detach from the substrate, forming debris. Wear debris of varying sizes could originate from both abrasive and fatigue mechanisms (Cowie et al., 2016), (Kocsis

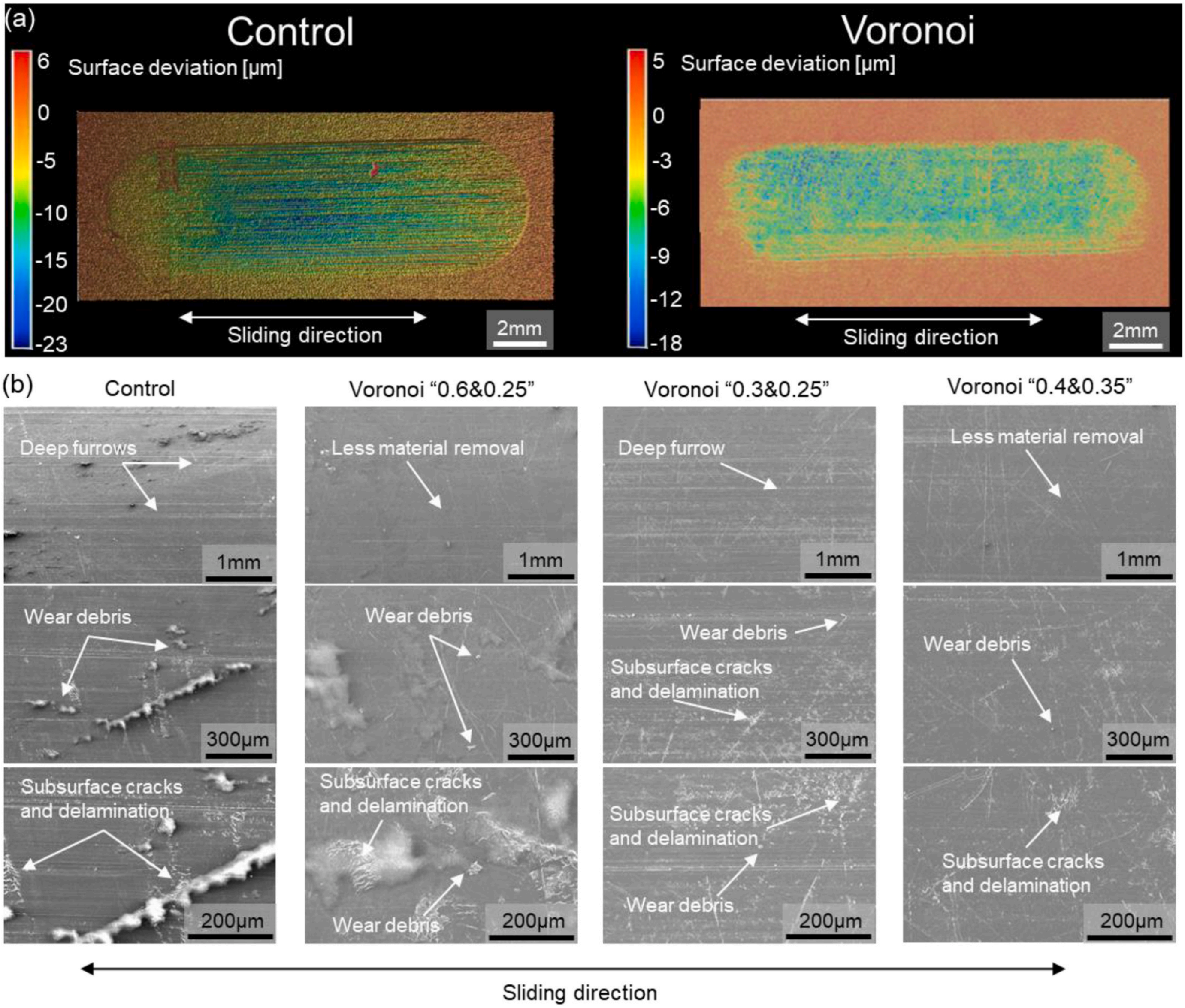

Fig. 9. Comparisons of representative UHMWPE disc surfaces after test. (a) Representative wear tracks scanned using optical profilometer. (b) Detailed wear surfaces observed using SEM.

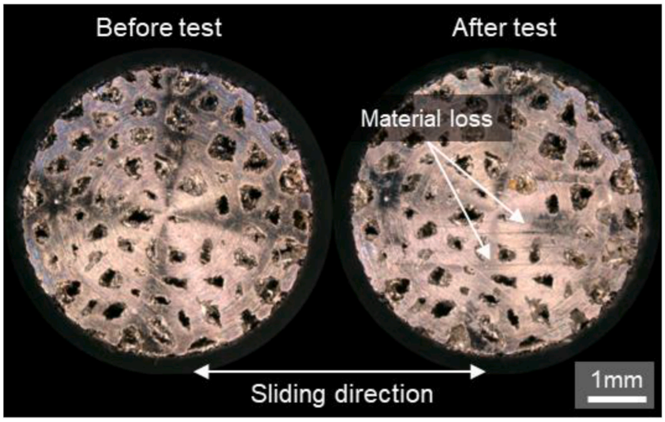

Fig. 10. Comparison of representative pin surfaces (Voronoi "0.5&0.2") before and after test.

et al., 2018). Hard debris worsens third-body wear, particularly in systems with poorly bonded metal particles, such as LPBF-fabricated components containing trapped powder. Therefore, cleaning and post-processing are needed to minimise interfacial contamination, as residual particles amplify abrasive damage and compromise wear resistance.

The observed material loss on the Ti6Al4V pin surfaces (Fig. 10) indicates that wear was not limited exclusively to the softer UHMWPE surfaces. Despite possessing significantly higher elastic modulus and surface hardness relative to UHMWPE, the Ti6Al4V pins exhibited visible wear. The presence of furrows suggests that hard asperities or wear debris particles caused local plastic deformation and material removal from the pin surface, characteristic of an abrasive wear mechanism. The bidirectional nature of material loss observed in this Ti6Al4V-UHMWPE tribological pairing aligns with the motion of the third-body abrasive particles during sliding contact. This finding is consistent with established literature reporting the relatively limited wear resistance of titanium alloys compared to Co-Cr alloys in orthopaedic applications, attributed to the lower surface hardness (Abd-Elaziem et al., 2024). Therefore, future investigations could focus

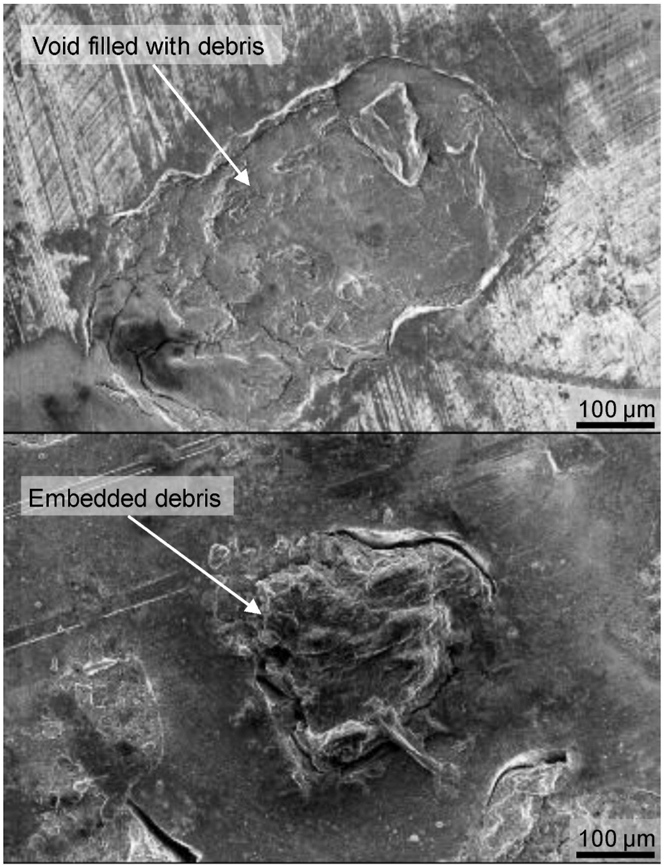

Fig. 11. SEM image of the pin specimen surface showing embedded polymer fragments.

on alternative metallic biomaterials with superior wear resistance characteristics and surface modification techniques such as physical vapor deposition coatings to improve the tribological properties of Ti6Al4V while maintaining its favourable biocompatibility.

Voronoi structures' potential to reduce friction and wear could make them suitable for improving artificial joint arthroplasty. One unique property of Voronoi structures is their inherent ability to conform to arbitrary shapes and surfaces, underscoring their suitability for articulating surfaces. Therefore, Voronoi structures emerge as a promising solution for replacing the metal surface of bearing components in artificial joint systems, such as shoulder implants. Besides, the geometry of Voronoi structures can be adapted for diverse loading conditions, thereby ensuring adequate load-bearing capacity and optimal tribological properties. Employing this principle could potentially mitigate the risk of aseptic loosening induced by wear debris and decrease the immune reactions in patients. As a result, the durability of the artificial joints could be enhanced, potentially diminishing the necessity for revision surgeries. However, this study has limitations that need further investigation. Future work could include experiments covering a wider range of parameter variations and larger sample sizes to verify the robustness of the findings. In addition, fatigue testing using a 5-axis simulator that accurately replicates the complex motions of human shoulder joints would provide results more reflective of clinical conditions.

5. Conclusion

This study investigated the tribological properties of Ti6Al4V Voronoi structures, manufactured using laser powder bed fusion (LPBF), when paired with ultra-high-molecular-weight polyethylene (UHMWPE) discs. The results of pin-on-disc (PoD) tests demonstrate that the Voronoi structures effectively reduce the static and dynamic coefficients of friction (COF) as well as the wear volume. Based on the results and their analysis, the following conclusions can be made:

- Voronoi structures exhibit highly variable geometries that can be precisely tuned by adjusting the seed point spacing and strut diameter. This adaptivity enables the relative density to be tailored and produces surface features (voids) that resemble the dimples in surface texturing. Consequently, the void dimensions and the contact area between the Voronoi pins and UHMWPE discs strongly depend on the design parameters.
- The application of Voronoi structures significantly reduces static COF, dynamic COF, and wear volume by 24.6 %, 29.4 %, and 51.2 %, respectively. The enhanced tribological properties are primarily attributable to the inherent porosity in Voronoi structures, which facilitates retaining synovial fluid and gathering wear debris. However, while these improvements are significant, no correlation was found between the geometric parameters and tribological properties.
- The wear track analysis confirmed the effective wear reduction of Voronoi structures, evidenced by the reductions in both the quantity and depth of the furrows on UHMWPE discs. The morphology of wear tracks confirmed abrasion as the primary wear mechanism.

In summary, this work enhances the understanding of the geometry and tribological properties of Voronoi structures. The findings of this study can contribute to the design and application of Voronoi structures for wear reduction, especially for the application of artificial joint arthroplasty. With their promising friction and wear reduction capabilities, Voronoi structures have the potential to be used for the next generation of artificial joint systems, potentially extending implant longevity and enhancing patient outcomes. However, further research, including fatigue testing and realistic multi-axis motion simulations, is needed to address the limitations of this study and ensure clinical applicability.

CRediT authorship contribution statement

Cong Hou: Writing – review & editing, Writing – original draft, Methodology, Investigation, Formal analysis. **István Nemes-Károly:** Writing – review & editing, Methodology, Investigation, Formal analysis. **Leonard Pastrav:** Writing – review & editing, Methodology. **Bey Vrancken:** Writing – review & editing, Supervision, Resources, Methodology, Conceptualization. **Gyorgy Kocsis:** Writing – review & editing, Supervision, Methodology, Funding acquisition, Conceptualization. **Gábor Szebényi:** Writing – review & editing, Writing – original draft, Supervision, Resources, Methodology, Funding acquisition, Formal analysis, Conceptualization. **Tibor Czigány:** Writing – review & editing, Supervision, Resources, Funding acquisition. **Kathleen Denis:** Writing – review & editing, Supervision, Resources, Methodology, Funding acquisition, Conceptualization.

Declaration of competing interest

The authors declare that they have no known competing financial interests or personal relationships that could have appeared to influence the work reported in this paper.

Acknowledgements

This work is supported by the CELSA Research Fund, Belgium and by Internal Funds KU Leuven, Belgium. This research is supported by the NRDI Office (OTKA K 138472). Gábor Szebényi acknowledges the financial support received through the János Bolyai Scholarship of the Hungarian Academy of Sciences and ÚNKP-23-5-BME-415 New National Excellence Program. The authors are grateful to ir. Kopila Gurung for her assistance in producing the samples.

Appendix A. Supplementary material

Table 4
Comparison of geometric properties of CAD geometry versus measured geometry of specimens, and corresponding results from PoD tests.

Sample	Seed point spacing (mm)	Strut diameter (mm)	Relative density of CAD geometry (%)	Void size in CAD geometry (μm)	Void size in specimen (μm)	Contact area of CAD geometry (mm^2)	Contact area of specimen (mm^2)	Static COF	Dynamic COF	Wear volume (mm^3)
control	–	–	100 %	–	–	19.6	–	0.24 ± 0.01	0.22 ± 0.02	1.14 ± 0.10
All Voronoi samples	–	–	–	–	–	–	–	0.18 ± 0.05	0.15 ± 0.04	0.56 ± 0.24
0.22 & 0.2	0.2	0.20	98.5 %	50.8 ± 23.5	197.1 ± 102.3	18.8	16.2 ± 1.8	0.16 ± 0.03	0.13 ± 0.04	0.44 ± 0.17
0.3 & 0.2	0.3	0.20	93.1 %	110.3 ± 50.6	197.6 ± 68.4	16.8	14.1 ± 0.6	0.18 ± 0.01	0.15 ± 0.03	0.57 ± 0.09
0.4 & 0.2	0.4	0.20	68.5 %	204.8 ± 87.8	270.1 ± 104.1	13.8	12.7 ± 2.5	0.19 ± 0.06	0.16 ± 0.03	0.49 ± 0.05
0.5 & 0.2	0.5	0.20	52.8 %	288.4 ± 131.7	297.6 ± 112.4	11.8	12.9 ± 0.3	0.25 ± 0.06	0.20 ± 0.03	0.80 ± 0.38
0.3 & 0.25	0.3	0.25	96.4 %	73.6 ± 31.0	195.4 ± 97.6	18.2	15.5 ± 0.8	0.21 ± 0.04	0.19 ± 0.03	0.81 ± 0.35
0.4 & 0.25	0.4	0.25	84.0 %	155.8 ± 70.1	174.5 ± 91.7	16.1	16.0 ± 1.7	0.18 ± 0.01	0.18 ± 0.02	0.67 ± 0.25
0.5 & 0.25	0.5	0.25	67.8 %	214.3 ± 113.0	220.8 ± 99.2	14.1	14.3 ± 1.0	0.19 ± 0.03	0.15 ± 0.03	0.63 ± 0.28
0.6 & 0.25	0.6	0.25	54.6 %	319.7 ± 142.3	340.3 ± 132.5	12.0	11.8 ± 1.0	0.17 ± 0.01	0.12 ± 0.04	0.52 ± 0.20
0.4 & 0.3	0.4	0.30	96.2 %	112.0 ± 52.5	148.5 ± 66.8	17.4	17.1 ± 0.0	0.17 ± 0.02	0.15 ± 0.02	0.52 ± 0.28
0.5 & 0.3	0.5	0.30	80.3 %	216.8 ± 91.5	194.8 ± 95.7	15.0	15.0 ± 1.5	0.23 ± 0.00	0.19 ± 0.02	0.71 ± 0.02
0.6 & 0.3	0.6	0.30	67.3 %	305.5 ± 147.5	284.9 ± 152.7	13.3	12.0 ± 0.2	0.15 ± 0.04	0.14 ± 0.05	0.50 ± 0.28
0.7 & 0.3	0.7	0.30	55.6 %	367.3 ± 171.7	328.9 ± 198.2	12.1	11.0 ± 1.6	0.21 ± 0.04	0.19 ± 0.03	0.46 ± 0.06
0.4 & 0.35	0.4	0.35	96.4 %	90.8 ± 51.3	164.7 ± 89.5	17.9	16.9 ± 1.4	0.17 ± 0.05	0.13 ± 0.07	0.79 ± 0.35
0.5 & 0.35	0.5	0.35	90.8 %	150.1 ± 77.9	209.0 ± 100.3	16.6	14.1 ± 1.3	0.21 ± 0.07	0.16 ± 0.04	0.42 ± 0.15
0.6 & 0.35	0.6	0.35	77.3 %	253.7 ± 123.6	232.1 ± 125.0	14.8	13.7 ± 0.5	0.14 ± 0.08	0.12 ± 0.07	0.52 ± 0.39
0.7 & 0.35	0.7	0.35	67.3 %	331.0 ± 152.5	293.4 ± 138.1	13.3	13.2 ± 0.0	0.16 ± 0.04	0.13 ± 0.05	0.36 ± 0.17

Table 5
Correlation coefficient for each pair of variables in tribological tests. The abbreviations of parameters are consistent with Fig. 8.

	SPS	SD	RD	VS	CA	SCOF	DCOF	W
W	−0.147	−0.106	0.049	−0.013	0.106	0.53	0.423	1
DCOF	−0.001	−0.107	−0.073	0.051	0.023	0.867	1	0.423
SCOF	0.001	−0.143	−0.129	0.08	0.013	1	0.867	0.53
CA	−0.626	0.018	0.765	−0.912	1	0.013	0.023	0.106
VS	0.638	−0.034	−0.807	1	−0.912	0.08	0.051	−0.013
RD	−0.767	0.068	1	−0.807	0.765	−0.129	−0.073	0.049
SD	0.567	1	0.068	−0.034	0.018	−0.143	−0.107	−0.106
SPS	1	0.567	−0.767	0.638	−0.626	0.001	−0.001	−0.147

Table 6
p-values for each pair of variables in correlation analysis. The abbreviations of parameters are consistent with Fig. 8. NA represent the p-value is not applicable.

	SPS	SD	RD	VS	CA	SCOF	DCOF	W
W	3.60E-01	5.11E-01	7.59E-01	9.38E-01	5.10E-01	3.69E-04	5.91E-03	NA
DCOF	9.93E-01	5.07E-01	6.49E-01	7.51E-01	8.86E-01	2.20E-13	NA	5.91E-03
SCOF	9.97E-01	3.73E-01	4.22E-01	6.17E-01	9.35E-01	NA	2.20E-13	3.69E-04
CA	1.22E-05	9.13E-01	5.59E-09	0.00E+00	NA	9.35E-01	8.86E-01	5.10E-01
VS	7.21E-06	8.31E-01	1.79E-10	NA	0.00E+00	6.17E-01	7.51E-01	9.38E-01
RD	5.13E-09	6.73E-01	NA	1.79E-10	5.59E-09	4.22E-01	6.49E-01	7.59E-01
SD	1.12E-04	NA	6.73E-01	8.31E-01	9.13E-01	3.73E-01	5.07E-01	5.11E-01
SPS	NA	1.12E-04	5.13E-09	7.21E-06	1.22E-05	9.97E-01	9.93E-01	3.60E-01

Data availability

Data will be made available on request.

References

Abd-Elaziem, W., Darwish, M.A., Hamada, A., Daoush, W.M., 2024. Titanium-based alloys and composites for orthopedic implants applications: a comprehensive review. Mater. Des. 241, 112850. https://doi.org/10.1016/j.matdes.2024.112850.

Abdelbary, A., 2021. Friction and wear of polymer and polymer composites. In: Jena, H., Katiyar, J.K., Patnaik, A. (Eds.), Tribology of Polymer and Polymer Composites for Industry 4.0. Springer, Singapore, pp. 33–54. https://doi.org/10.1007/978-981-16-3903-6_3.

Ajimotokan, H.A., 2024. Principles of frication, lubrication and wear. In: Ajimotokan, H. A. (Ed.), Principles and Applications of Tribology. Springer Nature Switzerland, Cham, pp. 7–28. https://doi.org/10.1007/978-3-031-57409-2_2.

Al-Shalawi, F.D., et al., 2023. Biomaterials as implants in the orthopedic field for regenerative medicine: metal versus synthetic polymers. Polymers 15 (12). https://doi.org/10.3390/polym15122601. Art. no. 12.

Allen, Q., Raeymaekers, B., 2020a. Surface texturing of prosthetic hip implant bearing surfaces: a review. J. Tribol. 143, 040801. https://doi.org/10.1115/1.4048409.

Allen, Q., Raeymaekers, B., 2020b. The effect of texture floor profile on the lubricant film thickness in a textured hard-on-soft bearing with relevance to prosthetic hip implants. J. Tribol. 143, 021801. https://doi.org/10.1115/1.4047753.

Almonti, D., Baiocco, G., Tagliaferri, V., Ucciardello, N., 2020. Design and mechanical characterization of voronoi structures manufactured by indirect additive manufacturing. Materials 13 (5). https://doi.org/10.3390/ma13051085. Art. no. 5.

Alvarez-Vera, M., et al., 2021. Tribological and microstructural characterization of laser microtextured CoCr alloy tested against UHMWPE for biomedical applications. Wear 477, 203819. https://doi.org/10.1016/j.wear.2021.203819.

Bergmann, G., et al., 2011. In vivo gleno-humeral joint loads during forward flexion and abduction. J. Biomech. 44 (8), 1543–1552. https://doi.org/10.1016/j.jbiomech.2011.02.142.

Braun, S., Schroeder, S., Mueller, U., Sonntag, R., Buelhoff, M., Kretzer, J.P., 2018. Influence of joint kinematics on polyethylene wear in anatomic shoulder joint arthroplasty. J. Shoulder Elb. Surg. 27 (9), 1679–1685. https://doi.org/10.1016/j.jse.2018.02.063.

Burstein, L., 2011. 3 - lubrication and roughness. In: Davim, J.P. (Ed.), Tribology for Engineers. Woodhead Publishing, pp. 65–120. https://doi.org/10.1533/9780857091444.65.

Chen, J., Gao, G., Fu, J., 2019. Clinical applications of UHMWPE in joint implants. In: Fu, J., Jin, Z.-M., Wang, J.-W. (Eds.), UHMWPE Biomaterials for Joint Implants: Structures, Properties and Clinical Performance. Springer Nature, Singapore, pp. 1–20. https://doi.org/10.1007/978-981-13-6924-7_1. Springer Series in Biomaterials Science and Engineering.

Chen, Y., Mao, Y., Yang, L., Wei, W., Meng, Q., Cai, J., 2022. A comprehensive review of factors affecting dynamic capillary effect in two-phase flow. Transport Porous Media 144 (1), 33–54. https://doi.org/10.1007/s11242-021-01723-x.

Choudhury, D., Rebenda, D., Sasaki, S., Hekrle, P., Vrbka, M., Zou, M., 2018. Enhanced lubricant film formation through micro-dimpled hard-on-hard artificial hip joint: an in-situ observation of dimple shape effects. J. Mech. Behav. Biomed. Mater. 81, 120–129. https://doi.org/10.1016/j.jmbbm.2018.02.014.

Connors, J.P., Stelzer, J.W., Garvin, P.M., Wellington, I.J., Solovyova, O., 2022. The role of the innate immune system in wear debris-induced inflammatory peri-implant osteolysis in total joint arthroplasty. Bioengineering 9 (12). https://doi.org/10.3390/bioengineering9120764. Art. no. 12.

Cowie, R.M., Carbone, S., Aiken, S., Cooper, J.J., Jennings, L.M., 2016. Influence of third-body particles originating from bone void fillers on the wear of ultra-high-molecular-weight polyethylene. Proc. Inst. Mech. Eng. [H] 230 (8), 775–783. https://doi.org/10.1177/0954411916651461.

Fryar, C., Carroll, M., Gu, Q., Afful, J., Ogden, C., 2021. Anthropometric reference data for children and adults: united States, 2015-2018. Vital Health Stat. 3 1–44. Avaliable: https://pubmed.ncbi.nlm.nih.gov/33541517/.

Goyal, V., Verma, G., 2024. Tribological behavior of direct metal laser sintering–manufactured Ti6Al4V alloy in different biofluids for orthopedic implants. J. Tribol. 146 (6). https://doi.org/10.1115/1.4064506.

Gundersen, T., et al., 2021. Annual Report 2021 Norwegian National Advisory Unit on Arthroplasty and Hip Fractures Norwegian Arthroplasty Register Norwegian Cruciate Ligament Register Norwegian Hip Fracture Register Norwegian Paediatric Hip Register. https://doi.org/10.13140/RG.2.2.34266.26566.

Hanaor, D.A.H., Gan, Y., Einav, I., 2016. Static friction at fractal interfaces. Tribol. Int. 93, 229–238. https://doi.org/10.1016/j.triboint.2015.09.016.

Hanniel, I., Elber, G., 2009. Computing the voronoi cells of planes, spheres and cylinders in R3. Comput. Aided Geomet. Des. 26 (6), 695–710. https://doi.org/10.1016/j.cagd.2008.09.010.

Hou, C., et al., 2022. Can 3d-printed voronoi structures reduce friction in orthopaedic implants? presented at the 27th Congress of the European Society of Biomechanics, Porto, Portugal, Jun 27. Available: https://lirias.kuleuven.be/retrieve/669888.

Hou, C., Sinico, M., Vrancken, B., Denis, K., 2024. Investigation of the laser powder bed fusion manufacturing process and quasi-static behaviour of Ti6Al4V voronoi structures. J. Mater. Process. Technol. 328, 118410. https://doi.org/10.1016/j.jmatprotec.2024.118410.

Igual Munoz, A., Espallargas, N., Mischler, S., 2020. Characterization of worn surfaces. In: Igual Munoz, A., Espallargas, N., Mischler, S. (Eds.), Tribocorrosion. Springer International Publishing, Cham, pp. 65–70. https://doi.org/10.1007/978-3-030-48107-0_7.

Ito, H., Kaneda, K., Yuhta, T., Nishimura, I., Yasuda, K., Matsuno, T., 2000. Reduction of polyethylene wear by concave dimples on the frictional surface in artificial hip joints. J. Arthroplast. 15 (3), 332–338. https://doi.org/10.1016/S0883-5403(00)90670-3.

Jiménez, A.-E., Bermúdez, M.-D., 2011. 2 - friction and wear. In: Davim, J.P. (Ed.), Tribology for Engineers. Woodhead Publishing, pp. 33–63. https://doi.org/10.1533/9780857091444.33.

Karunanithi, C., Natarajan, S., 2024. Surface characteristics of 3D printed PEEK polymer using atomic force microscopy. J. Mech. Behav. Biomed. Mater. 149, 106237. https://doi.org/10.1016/j.jmbbm.2023.106237.

Kim, I.-J., 2022a. Basic principles of tribology. In: Kim, I.-J. (Ed.), Engineering Metrology for Pedestrian Falls Prevention and Protection: Theories to Applications for Designing Safer Shoes and Floors. Springer International Publishing, Cham, pp. 53–116. https://doi.org/10.1007/978-3-030-95746-9_3.

Kim, I.-J., 2022b. Frictional behaviours and mechanisms. In: Kim, I.-J. (Ed.), Engineering Metrology for Pedestrian Falls Prevention and Protection: Theories to Applications for Designing Safer Shoes and Floors. Springer International Publishing, Cham, pp. 117–151. https://doi.org/10.1007/978-3-030-95746-9_4.

Kocsis, G., Payne, C.J., Wallace, A., McNally, D., 2018. Wear analysis of explanted conventional metal back polyethylene glenoid liners. Med. Eng. Phys. 59, 1–7. https://doi.org/10.1016/j.medengphy.2018.03.010.

Łapaj, Ł., Rozwalka, J., 2020. Retrieval analysis of TiN (titanium nitride) coated knee replacements: coating wear and degradation in vivo. J. Biomed. Mater. Res. B Appl. Biomater. 108 (4), 1251–1261. https://doi.org/10.1002/jbm.b.34473.

Li, Z., Feng, D., Li, B., Xie, D., Mei, Y., 2023. FDM printed MXene/MnFe2O4/MWCNTs reinforced TPU composites with 3D voronoi structure for sensor and electromagnetic shielding applications. Compos. Sci. Technol. 231, 109803. https://doi.org/10.1016/j.compscitech.2022.109803.

Liu, H., et al., 2022. High-quality surface smoothening of laser powder bed fusion additive manufacturing AlSi10Mg via intermittent electrochemical polishing. Surf. Coat. Technol. 443, 128608. https://doi.org/10.1016/j.surfcoat.2022.128608.

Lu, P., Wood, R.J.K., 2020. Tribological performance of surface texturing in mechanical Applications—A review. Surf. Topogr. Metrol. Prop. 8 (4), 043001. https://doi.org/10.1088/2051-672X/abb6d0.

Harris, W.H., 1995. The problem is osteolysis. Clin. Orthop. Relat. Res. 1976-2007. 311, 46 Feb. Avaliable: https://pubmed.ncbi.nlm.nih.gov/7634590.

Misir, A., Tokmak, T.T., Kizkapan, T.B., Uzun, E., Ozcamdali, M., 2019. Sex and side differences of three-dimensional glenoid anthropometric parameters in a normal Turkish population. Ann. Med. Res. 26 (10) Art. no. 10. https://doi.org/10.5455/annalsmedres.2019.07.377.

Nečas, D., et al., 2025. Frictional behaviour and surface topography evolution of DLC-coated biomedical alloys. Biosurface Biotribology 11 (1), e70004. https://doi.org/10.1049/bsb2.70004.

Nine, M.J., Choudhury, D., Hee, A.C., Mootanah, R., Osman, N.A.A., 2014. Wear debris characterization and corresponding biological response: artificial hip and knee joints. Materials 7 (2). https://doi.org/10.3390/ma7020980. Art. no. 2.

Niu, Y., Pang, X., Yue, S., Shangguan, B., Zhang, Y., 2021. The friction and wear behavior of laser textured surfaces in non-conformal contact under starved lubrication. Wear 476, 203723. https://doi.org/10.1016/j.wear.2021.203723.

Odehnal, L., et al., 2025. Tribological behaviour of additively manufactured Ti6Al4V with controlled surface structure: an application in small joint implants. Tribol. Int. 211, 110832. https://doi.org/10.1016/j.triboint.2025.110832.

Qiu, M., Chyr, A., Sanders, A.P., Raeymaekers, B., 2014. Designing prosthetic knee joints with bio-inspired bearing surfaces. Tribol. Int. 77, 106–110. https://doi.org/10.1016/j.triboint.2014.04.025.

R Core Team, R, 2021. A Language and Environment for Statistical Computing. R Foundation for Statistical Computing, Vienna, Austria. Accessed: May 16, 2023. Available: https://www.r-project.org/.

Ren, Y., et al., 2021. A review on tribology of polymer composite coatings. Friction 9 (3), 429–470. https://doi.org/10.1007/s40544-020-0446-4.

Sawano, H., Warisawa, S., Ishihara, S., 2009. Study on long life of artificial joints by investigating optimal sliding surface geometry for improvement in wear resistance. Precis. Eng. 33 (4), 492–498. https://doi.org/10.1016/j.precisioneng.2009.01.005.

Serdar, C.C., Cihan, M., Yücel, D., Serdar, M.A., 2021. Sample size, power and effect size revisited: simplified and practical approaches in pre-clinical, clinical and laboratory studies. Biochem. Med. 31 (1), 27–53. https://doi.org/10.11613/BM.2021.010502.

Shen, G., Fang, F., Kang, C., 2018. Tribological performance of bioimplants: a comprehensive review. Nanotechnol. Precis. Eng. NPE 1 (2), 107–122. https://doi.org/10.13494/j.npe.20180003.

Shen, G., Zhang, J.-F., Fang, F.-Z., 2019. In vitro evaluation of artificial joints: a comprehensive review. Adv. Manuf. 7 (1), 1–14. https://doi.org/10.1007/s40436-018-00244-z.

Stewart, T.D., 2010. Tribology of artificial joints. Orthop. Traumatol. 24 (6), 435–440. https://doi.org/10.1016/j.mporth.2010.08.002.

Tanemura, M., Ogawa, T., Ogita, N., 1983. A new algorithm for three-dimensional voronoi tessellation. J. Comput. Phys. 51 (2), 191–207. https://doi.org/10.1016/0021-9991(83)90087-6.

Thrush, S.J., et al., 2021. Wear mechanisms of a sintered tribofilm in boundary lubrication regime. Wear 482–483, 203932.. https://doi.org/10.1016/j.wear.2021.203932.

Wang, C., et al., 2022. Enhanced biotribological and anticorrosion properties and bioactivity of Ti6Al4V alloys with laser texturing. ACS Omega 7 (35), 31081–31097. https://doi.org/10.1021/acsomega.2c03166.

Wei, X., et al., 2016. Surface modification of co–cr–mo implant alloy by laser interference lithography. Tribol. Int. 97, 212–217. https://doi.org/10.1016/j.triboint.2016.01.039.

Contact between surfaces. In: Williams, J. (Ed.), 2005. Engineering Tribology. Cambridge University Press, Cambridge, pp. 73–131. https://doi.org/10.1017/CBO9780511805905.004.

Wu, Z., Narra, S.P., Rollett, A., 2020. Exploring the fabrication limits of thin-wall structures in a laser powder bed fusion process. Int. J. Adv. Manuf. Technol. 110 (1), 191–207. https://doi.org/10.1007/s00170-020-05827-4.

Xue, M., Chen, X., Ji, X., Xie, X., Chao, Q., Fan, G., 2023. Effect of particle size distribution on the printing quality and tensile properties of Ti-6Al-4V alloy produced by LPBF process. Metals 13 (3). https://doi.org/10.3390/met13030604. Art. no. 3.

Zhai, W., et al., 2021. Recent progress on wear-resistant materials: designs, properties, and applications. Adv. Sci. 8 (11), 2003739. https://doi.org/10.1002/advs.202003739.

Zhang, J., Li, B., 2022. The influence of laser powder bed fusion (L-PBF) process parameters on 3D-Printed quality and stress–strain behavior of high-entropy alloy (HEA) rod-lattices. Metals 12 (12). https://doi.org/10.3390/met12122109. Art. no. 12.

Zhang, H., Qin, L., Hua, M., Dong, G., Chin, K.-S., 2015. A tribological study of the petaloid surface texturing for co–cr–mo alloy artificial joints. Appl. Surf. Sci. 332, 557–564. https://doi.org/10.1016/j.apsusc.2015.01.215.

Zhao, Z., Li, J., Yao, D., Wei, Y., 2022. Mechanical and permeability properties of porous scaffolds developed by a voronoi tessellation for bone tissue engineering. J. Mater. Chem. B 10 (46), 9699–9712. https://doi.org/10.1039/D2TB01478E.